WASHINGTON STATE UNIVERSITY
Institute for Shock Physics

This publication is based upon work performed at the Dynamic Compression Sector, which is operated by Washington State University under the U.S. Department of Energy (DOE)/National Nuclear Security Administration award no. DE-NA0003957.

Dynamic high pressure phase transformation of ZrW_2O_8

Bishop, S. R., D. R. Lowry, A. S. Peretti, P. Kalita, M. D. Knudson, A. Sarracino, J. T. Mahaffey, and S. E. Murray

DOI: 10.1063/5.0147942

Published: June 2023

AIP Advances

RESEARCH ARTICLE | JUNE 01 2023

Dynamic high pressure phase transformation of ZrW_2O_8

Sean R. Bishop ; Daniel R. Lowry ; Amanda S. Peretti ; Pat Kalita ; Marcus D. Knudson ; Alex Sarracino ; Jacob T. Mahaffey ; Shannon E. Murray

AIP Advances 13, 065101 (2023)
https://doi.org/10.1063/5.0147942

Dynamic high pressure phase transformation of ZrW_2O_8

Cite as: AIP Advances 13, 065101 (2023); doi: 10.1063/5.0147942
Submitted: 8 March 2023 • Accepted: 13 May 2023 •
Published Online: 1 June 2023

Sean R. Bishop,[a] Daniel R. Lowry, Amanda S. Peretti, Pat Kalita, Marcus D. Knudson, Alex Sarracino, Jacob T. Mahaffey, and Shannon E. Murray

AFFILIATIONS

Sandia National Laboratories, Albuquerque, New Mexico 87123, USA

[a]Author to whom correspondence should be addressed: srbisho@sandia.gov

ABSTRACT

Phase transformations under high strain rates (dynamic compression) are examined *in situ* on ZrW_2O_8, a negative thermal expansion ternary ceramic displaying polymorphism. Amorphization, consistent with prior quasi-static measurements, was observed at a peak pressure of 3.0 GPa under dynamic conditions, which approximate those expected during fabrication. Evidence of partial amorphization was observed at lower pressure (1.8 GPa) that may be kinetically restrained by the short (<~150 ns) time scale of the applied high pressure. The impact of kinetics of pressure-induced amorphization from material fabrication methods is briefly discussed.

INTRODUCTION

Dynamic compression coupled with x-ray diffraction (XRD) is a technique that was recently developed at the Dynamic Compression Sector (DCS) using the Advanced Photon Source at Argonne National Laboratory. The DCS has been used to explore phase transitions under very high strain rates and pressures by launching an impactor from a powder gun at a sample while measuring XRD on the sample at sub-microsecond time scales.[1,2] This measurement technique is key to understanding the behavior of compression-driven phase transformations, their pathways, and kinetics. Prior dynamic compression XRD work has focused on monatomic solids,[1] with only limited work on single crystal binary materials.[3,4] In this paper, we examine the dynamic compression XRD response of ternary, polycrystalline cubic ZrW_2O_8, which exhibits negative thermal expansion[5] and at room temperature is meta-stable.

Negative thermal expansion materials are attractive for tuning the thermal expansion of composites.[6] The cubic phase of ZrW_2O_8 is typically fabricated by thermal quenching from above the cubic phase formation temperature of 1108 °C[7] or through decomposition of a chemically prepared hydrated phase at 600 °C.[8] Upon heating cubic ZrW_2O_8 from room temperature, an order–disorder transition occurs at ~155 °C from $P2_13$ (α-ZrW_2O_8) to $Pa\bar{3}$ (β-ZrW_2O_8) space groups. The material decomposes to ZrO_2 and WO_3 at ~800 °C,[5] indicating metastability at room temperature.[9] At room temperature, with the isostatic pressure increasing to ~0.2 GPa, an orthorhombic phase (γ-ZrW_2O_8; $P2_12_12_1$) is formed, followed by pressure-induced amorphization (PIA) at 1.5–3.5 GPa, which is retained upon release of pressure.[10–13] Annealing the PIA phase at 600 °C in ambient pressure re-forms the cubic phase,[14] and annealing at 769 °C and 2.2 GPa forms the hexagonal α-U_3O_8 ($P\bar{6}2m$) phase, which may also be formed from the $Pa\bar{3}$ phase at 1.2 GPa and 524 °C, which are retained upon return to ambient in both cases.[11]

The above-mentioned discussion highlights the variety of phases that are found in this material under different thermal and pressure environments. Thus far, all pressure measurements have been performed under quasistatic conditions, and this paper reports the crystallographic response to high pressure at a high strain rate. Phase changes observed in quasi-static testing are not necessarily expected to be the same in dynamic compression due to the short time scale (<1 μs) of applied pressure, limiting diffusion[2] in combination with the abrupt increase in pressure that may only be a few lattice planes wide in front of the shock wave.[15] Furthermore, the relatively low pressures needed for a phase change present challenges for materials processing, which often have dynamic loads, for

example, in coatings deposited via kinetic spray (e.g., cold spray or aerosol deposition) where supersonic collisions of feedstock powder may result in very large stress during particle impact as well as very large residual stress within the coating.[16,17] Indeed, previous researchers have reported amorphization during sample grinding with a mortar and pestle.[10] The dynamic compression study carried out here is thus expected to approximate possible stress conditions found during fabrication.

EXPERIMENTAL

ZrW_2O_8 powder was fabricated using mixed oxides of ZrO_2 and WO_3 (US Research Nanomaterials, Inc.) ball milled in water, dried, and then pressed into pellets that were subsequently calcined at 1160 °C for 4 h on top of a Pt sheet to avoid reactivity with the alumina setter. Samples were quenched to room temperature from calcination conditions by pushing them out of the tube furnace quickly to a fan blowing air. After calcination, the pellets were ground and ball milled again and then uniaxially (69 MPa) and isostatically (207 MPa) pressed and sintered under the same conditions as calcination followed by quenching. The speed of sound measurements was performed using the pulse-echo method. The density was measured using the Archimedes method.

Samples for dynamic compression measurements were composed of ~15 mm diameter slices from a single pellet that were bonded to a polymethylpentene window (trade name TPX®, Mitsui Chemicals, Inc.)[18] (2.1 mm thick by 19.05 mm diameter) using AngstromBond AB9110LV. The pellet and TPX were sanded flat to 12.6 μm and finished with SiC paper before bonding. After bonding, the pellet was sliced using a diamond saw and sanded using up to 35 μm SiC paper with water to a final thickness of 50–60 μm, enabling sufficient x-ray transmission (e.g., >100 μm thickness was experimentally found to be too absorbing). This process was repeated for all the tested samples from the same pellet. For shock measurements, polycarbonate impactors were accelerated to 0.7–1.2 km/s using a single stage powder gun. A focused pink x-ray beam, with the peak intensity at 36 keV, was used for single-pulse XRD images (~100 ps duration). A four-image XRD detector allows for the study of the temporal evolution of structure during shock compression by recording four XRD snapshots.[1] We used photon Doppler velocimetry (PDV)[19] with a 1550 nm wavelength probe laser with a probe diameter of 1 mm. PDV data were analyzed using the Sandia InfraRed HEtrodyne aNalysis (SIRHEN)[20] software found in the SMASH toolbox.[21] A Fourier transform window of 30 ns with a step size of 5 ns was utilized to accurately measure the acceleration shortly after impact. XRD powder diffraction files (PDFs) used in analysis are 04-009-7348 for α-ZrW_2O_8, 01-073-8457 for γ-ZrW_2O_8, 01-083-0944 for m-ZrO_2 (monoclinic), and 01-083-0950 for m-WO_3 (monoclinic). Structure refinement and whole pattern fitting methods using Topas software (Bruker) was used to estimate the lattice parameters. The initial peak shape function was determined by refinement of the standard Si pattern. Analysis of the XRD data released the refinement of the structure scale factors, lattice parameters for the α- and γ-ZrW_2O_8 phases, and Gaussian and Lorentzian crystallite terms for peak broadening. For structural refinement, composition from the PDFs mentioned above was included and kept constant during analysis, while for whole pattern fitting, this information was not included.

RESULTS

The composition of the two ~6 mm thick × 13 mm diameter pellets after quench sintering is 95% α-ZrW_2O_8 with impurity phases of ZrO_2, WO_3, and γ-ZrW_2O_8, identified using powder XRD prior to studies at the DCS. The density is 4.494 g/cm^3 or 89% of the theoretical value of 5.071 g/cm^3.[22] The average longitudinal and transverse speed of sounds of the two pellets is 4.177 and 2.413 km/s, respectively. This translates to a Young's elastic modulus of 65 GPa, bulk modulus of 75 GPa, shear modulus of 26 GPa, and Poisson's ratio of 0.2, and this is comparable to the wide range bulk modulus of 48–74 GPa and Poisson's ratio of 0.30 previously reported.[14,23] The sample porosity is expected to have reduced the moduli, as compared to a dense sample. Samples tested at DCS were sliced from one of the pellets, as described in the experimental section. The microstructure of a piece of the sample prepared from the other pellet is shown in Fig. 1. ~8% porosity was estimated using ImageJ analysis software,[24] slightly lower than the Archimedes estimated porosity, likely from the expected underestimation in image analysis. Approximately spherical pores (consistent with the high temperature sintering, near the melting point of ~1231 °C[7]) with sizes of ~1 to 8 μm are observed, with some sub-micron porosity evident as well. Micro-cracking was observed, as shown in the figure, which likely occurred from stresses created during quenching from high temperature sintering. A grain size of ~10–30 μm is estimated from backscatter electron micrographs.

An example of the velocity profile measured at the back of the sample using PDV analysis for an impactor velocity of 1.222 km/s is shown in Fig. 2. At impact, a large stress is generated at the sample surface, which progresses as a shockwave through the sample. The shockwave travels across the sample in ~13 ns (based on the speed of sound and sample thickness), after which there is a sudden initial steep rise in the measured velocity as the PDV probe records sample movement at the sample–window interface. As time progresses, the shockwave bounces between sample interfaces with the window and impactor, resulting in an observed characteristic feature at ~500 m/s (one of the reflections off the sample–window interface).

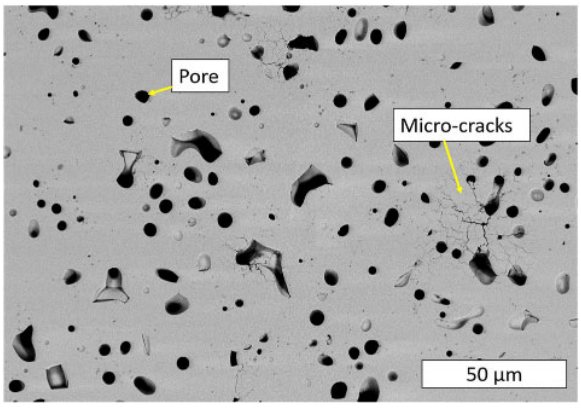

FIG. 1. Electron backscatter image of the polished sample showing porosity and micro-cracks.

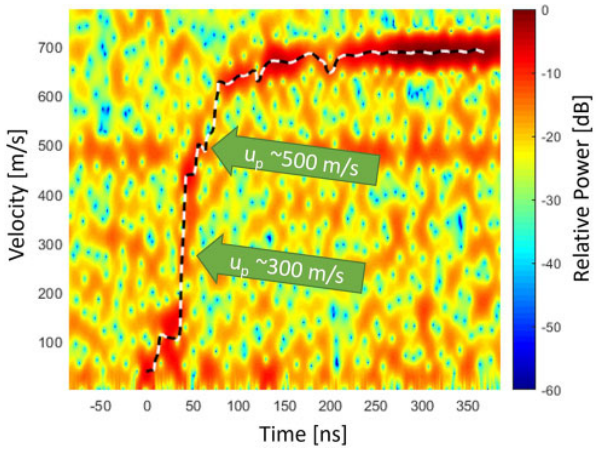

FIG. 2. Example of the PDV response during dynamic compression for a sample impacted at 1.222 km/s. The dashed line is a fit to the analyzed data. Arrows indicate velocity points of the expected wave reflections off the sample/window interface based on elastic properties.

At times >~150 ns, in these measurements, the sample experiences a quasi-static pressure and temperature (i.e., quasi-constant velocity in the figure) for tens of ns, which is when the sample is uniformly compressed between the impactor and window. Using the elastic properties derived from the speed of sound measurements, the velocities (u_p) for the wave reflections off the back of the sample were estimated and are indicated in Fig. 2. The second reflection matches well with a feature in the PDV analysis. Unfortunately, a relatively low signal-to-noise ratio was observed in the measurements, likely from the very thin samples required to achieve adequate x-ray transmission for structural analysis. As a result, the first characteristic reflection is not observed in the patterns. Given the agreement in the estimated wave reflection timing and the characteristic in the PDV described above, the response of the samples was deemed to be elastic under these conditions. The pressure estimated for the sample at impact, using impedance matching based on the elastic properties of the sample and the Hugoniot of the impactor and window, and at 1.222 km/s impactor velocity (Fig. 2) is 3.1 GPa.[25] The pressure estimated from the Hugoniot of the impactor and window at the quasi-steady-state pressure and temperature generated from ring-down (i.e., the plateau in velocity at time later than 150 ns in Fig. 2) is 2.0 GPa.

The before impact (left) XRD image in Fig. 3 shows clear diffraction (Debye) spots from the large grains in the sample with some characteristic rings for TPX at a low angle (right-side of the image) and, after impact, a loss of diffraction lines from the sample, consistent with amorphization. All four XRD images, collected sequentially at 153 ns intervals, after impact showed the same response as the after-impact image in the figure. The integrated XRD images are shown in Fig. 4 for a second sample measured at a nearly identical impact velocity of 1.221 km/s and thus similar impact pressure. The diffraction peaks before impact (0) are consistent with the α-ZrW_2O_8 phase, with low angle peaks consistent with TPX (shown by vertical dashed lines). After impact (1–4), a broad increase in

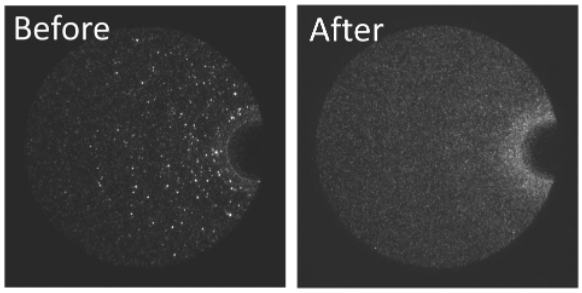

FIG. 3. XRD image before (left) and <153 ns after (right) impact for the sample impacted at 1.222 km/s.

intensity is observed, consistent with sample amorphization. Both measurements (1.221 and 1.222 km/s impact velocity) showed similar results, demonstrating that the amorphization is consistently observed. Due to challenges in timing interpretation, the exact start of x-ray imaging is not clear but is estimated to be within ~150 ns of impact. The peak pressure at which amorphization during dynamic compression occurred (3.1 GPa) is within PIA pressures reported from quasistatic measurements described in the introduction.

Turning now to pressures close to the threshold expected to result in PIA, two experiments with nearly identical impactor velocities of 0.731 and 0.741 km/s were used, resulting in an estimated peak pressure (at impact) of 1.8 GPa with a quasi-steady-state pressure of 1.0 GPa (at the plateau in velocity in PDV). After impact, diffraction peaks clearly remain, although a broadening is observed, as shown in Fig. 5. Broadening may arise from partial amorphization that is consistent with the lowest reported PIA of 1.5 GPa described in the introduction, which is lower than the estimated peak stress of 1.8 GPa here. Within ~150 ns, the lower 1.0 GPa quasi-steady-state pressure is reached, at which point PIA is not expected, indicating that the kinetics of amorphization are too slow for this time frame. As indicated in the introduction, high compressive pressures can occur in fabrication methods. This research has shown that the time

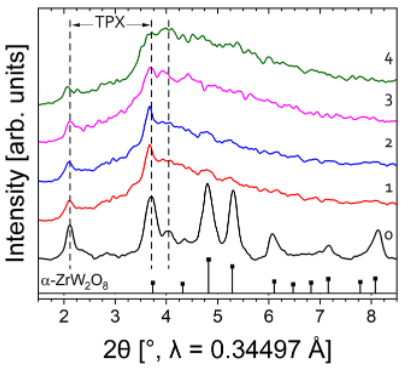

FIG. 4. XRD patterns before (0) and after (1–4 sequentially in time, 153 ns apart) impact for an impactor velocity of 1.221 km/s corresponding to an approximate maximum pressure of 3.1 GPa. Vertical dashed and solid lines show expected peak positions for TPX and ZrW_2O_8, respectively.

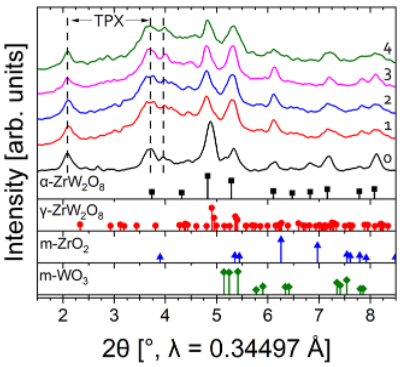

FIG. 5. XRD patterns before (0) and after (1–4 sequentially in time, 153 ns apart) impact for an impactor velocity of 0.731 km/s, corresponding to an approximate maximum pressure of 1.8 GPa. Vertical dashed and solid lines show expected peak positions for TPX and indicated phases, respectively.

frame of applied pressure plays an important role in amorphization and, for example, the short stress pulses expected in ball milling and spraying would require a higher stress for amorphization than the quasistatic case.

For the diffraction peaks, while there are some relative changes in peak intensity (likely from re-orientation of grains with respect to the x-ray source and detector from sample movement during shock), there are no obvious secondary phases formed (e.g., ZrO_2 or WO_3), which would indicate decomposition of the metastable material. Unfortunately, changes in the phase fraction of γ-ZrW_2O_8 and α- ZrW_2O_8 cannot be reliably determined here due to the similarity in XRD patterns coupled with the low XRD signal-to-noise ratio for these samples at the DCS. As noted in the introduction, formation of γ is expected to be above 0.2 GPa. Similar behavior was observed in the second sample, as shown in Fig. 6 (although a timing issue led to only one of the post-impact XRD images occurring within the experimental time frame). Finally, a decrease in the lattice parameter

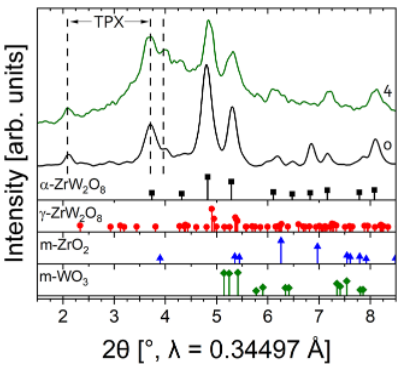

FIG. 6. XRD patterns before (0) and after (4) impact for an impactor velocity of 0.74 km/s, corresponding to an approximate maximum pressure of 1.8 GPa. Vertical dashed and solid lines show expected peak positions for TPX and indicated phases, respectively.

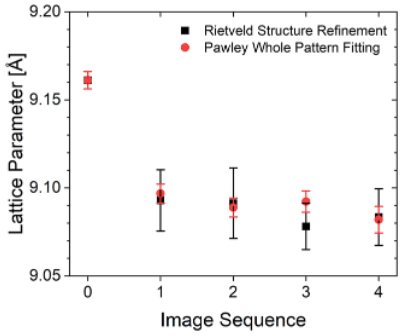

FIG. 7. Lattice parameter estimates from two different fitting techniques for the low velocity samples before (0) and after (1–4) impact.

after impact was observed for the two lower impact velocities during the DCS measurement, as expected from the applied compressive stress, which is shown in Fig. 7. However, after the initial decrease immediately following impact, the lattice parameter remains constant, within the error of the two refinement methods, for the four XRD images, consistent with the quasi-steady-state-pressure applied over this time frame. The initial lattice parameter shown in Fig. 7 is 9.161 (2) Å, which is similar to the 9.1575 (2) Å reported previously for α-ZrW_2O_8.[5]

CONCLUSIONS

α-ZrW_2O_8 samples were examined under dynamic compression with *in situ* XRD at the DCS. Amorphization was observed at a peak pressure of 3.0 GPa and is consistent with quasi-static measurements. At 1.8 GPa, evidence of partial amorphization was observed that may be kinetically restrained by the short (<~150 ns) time scale of the applied high pressure. This result has implications in material processing, where the short stress pulses expected in, for example, ball milling and kinetic spray would require a higher stress for amorphization than the quasistatic case.

ACKNOWLEDGMENTS

The authors thank Thomas Diebold and Luis Juaregui at Sandia National Laboratories for their assistance with sample preparation and electron microscopy.

This article has been authored by an employee of National Technology and Engineering Solutions of Sandia, LLC under Contract No. DE-NA0003525 with the U.S. Department of Energy (DOE). The employee owns all right, title, and interest in and to the article and is solely responsible for its contents. The United States Government retains and the publisher, by accepting the article for publication, acknowledges that the United States Government retains a non-exclusive, paid-up, irrevocable, world-wide license to publish or reproduce the published form of this article or allow others to do so, for United States Government purposes.

The DOE will provide public access to these results of federally sponsored research in accordance with the DOE Public Access Plan https://www.energy.gov/downloads/doe-public-access-plan.

This publication is based on the work performed at the Dynamic Compression Sector, which is operated by Washington State University under U.S. Department of Energy (DOE)/National Nuclear Security Administration Award No. DE-NA0003957. This research used the resources of the Advanced Photon Source, a DOE Office of Science User Facility operated for the DOE Office of Science by Argonne National Laboratory under Contract No. DE-AC02-06CH11357.

AUTHOR DECLARATIONS

Conflict of Interest

The authors declare no conflicts of interest.

Author Contributions

S.R.B. and D.R.L. contributed equally to this work.

Sean R. Bishop performed analysis and manuscript writing, Daniel R. Lowry performed XRD analysis and experiments at DCS, Amanda S. Peretti performed sample fabrication, Patricia Kalita and Marcus D. Knudson assisted with mechanical shock analysis, Alex Sarracino performed analysis of velocimetry, Jacob T. Mahaffey and Shannon E. Murray formulated the idea and assisted in materials property analysis.

Sean R. Bishop: Conceptualization (equal); Formal analysis (equal); Methodology (equal); Writing – original draft (equal); Writing – review & editing (equal). **Daniel R. Lowry**: Formal analysis (equal); Investigation (equal); Methodology (equal); Writing – original draft (equal); Writing – review & editing (equal). **Amanda S. Peretti**: Investigation (equal). **Pat Kalita**: Formal analysis (equal); Methodology (equal); Writing – review & editing (equal). **Marcus D. Knudson**: Formal analysis (equal); Methodology (equal); Writing – review & editing (equal). **Alex Sarracino**: Formal analysis (equal). **Jacob T. Mahaffey**: Conceptualization (equal); Methodology (equal). **Shannon E. Murray**: Conceptualization (equal); Methodology (equal); Writing – review & editing (equal).

DATA AVAILABILITY

The data that support the findings of this study are available from the corresponding author upon reasonable request.

REFERENCES

[1] P. Kalita, P. Specht, S. Root, N. Sinclair, A. Schuman, M. White, A. L. Cornelius, J. Smith, and S. Sinogeikin, Phys. Rev. Lett. **119**, 255701 (2017).
[2] M. G. Newman, R. G. Kraus, M. C. Akin, J. V. Bernier, A. M. Dillman, M. A. Homel, S. Lee, J. Lind, J. L. Mosenfelder, D. C. Pagan, N. W. Sinclair, and P. D. Asimow, Geophys. Res. Lett. **45**, 8129, https://doi.org/10.1029/2018gl077996 (2018).
[3] P. Kalita, J. Brown, P. Specht, S. Root, M. White, and J. S. Smith, Phys. Rev. B **102**, 060101 (2020).
[4] S. J. Tracy, S. J. Turneaure, and T. S. Duffy, Sci. Adv. **6**, eabb3913 (2020).
[5] J. S. O. Evans, T. A. Mary, T. Vogt, M. A. Subramanian, and A. W. Sleight, Chem. Mater. **8**, 2809 (1996).
[6] A. W. Sleight, Annu. Rev. Mater. Sci. **28**, 29 (1998).
[7] L. L. Y. Chang, M. G. Scroger, and B. Phillips, J. Am. Ceram. Soc. **50**, 211 (1967).
[8] C. Closmann, A. W. Sleight, and J. C. Haygarth, J. Solid State Chem. **139**, 424 (1998).
[9] A. K. Arora, V. S. Sastry, P. C. Sahu, and T. A. Mary, J. Phys.: Condens. Matter **16**, 1025 (2004).
[10] C. A. Perottoni and J. A. H. d. Jornada, Science **280**, 886 (1998).
[11] A. Grzechnik, W. A. Crichton, K. Syassen, P. Adler, and M. Mezouar, Chem. Mater. **13**, 4255 (2001).
[12] T. Varga, A. P. Wilkinson, A. C. Jupe, C. Lind, W. A. Bassett, and C.-S. Zha, Phys. Rev. B **72**, 024117 (2005).
[13] D. A. Keen, A. L. Goodwin, M. G. Tucker, M. T. Dove, J. S. O. Evans, W. A. Crichton, and M. Brunelli, Phys. Rev. Lett. **98**, 225501 (2007).
[14] R. F. L. Lorenzi, J. E. Zorzi, and C. A. Perottoni, J. Non-Cryst. Solids **403**, 102 (2014).
[15] F. Langenhorst and A. Deutsch, Elements **8**, 31 (2012).
[16] S. Suresh, S.-W. Lee, M. Aindow, H. D. Brody, V. K. Champagne, and A. M. Dongare, Acta Mater. **182**, 197 (2020).
[17] A. Vackel, J. Therm. Spray Technol. **30**, 584 (2021).
[18] S. Root, T. R. Mattsson, K. Cochrane, R. W. Lemke, and M. D. Knudson, J. Appl. Phys. **118**, 205901 (2015).
[19] D. H. Dolan, Rev. Sci. Instrum. **91**, 051501 (2020).
[20] I. Dolan, H. Daniel, and T. Ao, Technical Report No. SAND2010-3628 (Sandia National Laboratories, 2010). DOI:
[21] D. Dolan, Sandia Matlab Analysis Hierarchy toolbox v. 1.0, 2016.
[22] T. A. Mary, J. S. O. Evans, T. Vogt, and A. W. Sleight, Science **272**, 90 (1996).
[23] G. Ernst, C. Broholm, G. R. Kowach, and A. P. Ramirez, Nature **396**, 147 (1998).
[24] ImageJ Version 1.53. NIH, 2022.
[25] G. E. Duvall and R. A. Graham, Rev. Mod. Phys. **49**, 523 (1977).